

Anisotropic Exchange Spin Model to Investigate the Curie Temperature Dispersion of Finite-Size $L1_0$ -FePt Magnetic Nanoparticles

Kohei Ochiai,¹ Tomoyuki Tsuyama,¹ Sumera Shimizu,¹ Lei Zhang,² Jin Watanabe,² Fumito Kudo,² Jian-Gang Zhu,^{3,4,5} and Yoshishige Okuno¹

¹*Resonac Corporation, Research Center for Computational Science and Informatics, 8, Ebisu-cho, Kanagawa-ku, Yokohama, Kanagawa. 221-8517, Japan*

²*Resonac Hard Disk Corporation, Research & Development Center, 5-1, Yawatakaigan-dori, Ichihara, Chiba, 290-0067, Japan*

³*Data Storage Systems Center, Carnegie Mellon University, Pittsburgh, PA 15213, USA*

⁴*Electrical and Computer Engineering Department, Carnegie Mellon University, Pittsburgh, PA 15213, USA*

⁵*Materials Science and Engineering Department, Carnegie Mellon University, Pittsburgh, PA 15213, USA*

(*Electronic mail: ochiai.kohei.xiqrk@resonac.com)

(Dated: 24 February 2025)

We developed an anisotropic spin model that accounts for magnetic anisotropy and evaluated the Curie temperature (T_c) dispersion due to finite size effects in $L1_0$ -FePt nanoparticles. In heat-assisted magnetic recording (HAMR) media, a next-generation magnetic recording technology, high-density recording is achieved by locally heating $L1_0$ -FePt nanoparticles near their T_c and rapidly cooling them. However, variations in T_c caused by differences in particle size and shape can compromise recording stability and areal density capacity, making the control of T_c dispersion critical. In this study, we constructed atomistic LLG models to explicitly incorporate the spin exchange anisotropy of $L1_0$ -FePt, based on parameters determined by first-principles calculations. Using this model, we evaluated the impact of particle size on T_c dispersion. As a result, (1) the T_c dispersion critical to the performance of HAMR can be reproduced, whereas it was previously underestimated by isotropic models and (2) approximately 70% of the experimentally observed T_c dispersion can be attributed to particle size effects. This research highlights the role of exchange anisotropy in amplifying finite-size effects and underscores the importance of size control in HAMR media.

I. INTRODUCTION

In recent years, with the rapid expansion of cloud services, big data, and AI, the volume of data generated worldwide is predicted to rise dramatically¹. Consequently, from the viewpoint of cost and energy efficiency per bit, there is a strong demand for increasing the capacity and density of storage systems geared toward data centers. Conventional magnetic recording techniques face limits in recording density, commonly called the "magnetic trilemma (Trilemma)." As a next-generation technology, Heat-Assisted Magnetic Recording (HAMR) has attracted considerable attention^{2,3}. By locally heating a nanoparticle to near its Curie temperature and rapidly cooling it, HAMR enables high-density recording while maintaining large magnetic anisotropy.

A key parameter that influences HAMR performance is the magnetic particles' Curie temperature (T_c). Materials such as $L1_0$ -phase FePt (hereafter referred to as $L1_0$ -FePt), with extremely large magnetic anisotropy constants, are especially promising⁴⁻⁶. However, experimental studies report substantial variation in T_c due to particle size, shape, and degree of order⁷⁻¹². This spread in T_c can undermine recording stability and degrade the signal-to-noise ratio (SNR) by causing mismatch between the writing temperature and each particle's actual Curie temperature^{13,14}. Moreover, there are reports that T_c dispersion is crucial for determining areal density capability (ADC)¹⁵, underscoring the need to control it in HAMR media design. Although T_c dispersion's impact on SNR and ADC is understood, which parameters predom-

inantly create such dispersion remains unclear. The strong exchange anisotropy of the layered $L1_0$ -FePt structure^{16,17} and real particle shapes have not been fully integrated into theoretical models. While some prior studies link particle-size distribution to T_c variation¹⁰, it has also been noted that single-domain or isotropic-mesh simulations cannot capture exchange anisotropy effects effectively¹⁸.

Against this background, the this study aims to incorporate Fe-Fe interactions (particularly those arising from exchange anisotropy due to the layered structure) obtained from first-principles calculations (DFT) into an atomistic-scale spin model. Furthermore, we conduct numerical simulations accounting for realistic particle-size distribution. Specifically, we first use a modified simple-cubic (modified-sc) model¹⁰ to assess how T_c drops with particle size. Next, we build an anisotropic spin model incorporating $L1_0$ -FePt exchange parameters to reproduce and verify T_c dispersion arising from particle-size distribution quantitatively. This approach captures the T_c dispersion more accurately previous isotropic models often underestimate it-and can explain approximately 70% of experimentally reported values. We also propose design strategies for mitigating T_c dispersion in HAMR media.

II. THEORIES

This section describes the theoretical models and methods employed to evaluate the magnetic properties of $L1_0$ -FePt nanoparticles quantitatively. We first construct an atomistic

spin model incorporating the markedly different exchange interactions operating within and between atomic layers (intra-layer vs. interlayer). We then outline how we extracted the exchange interaction constants using first-principles (DFT) calculations. In addition, to facilitate a more straightforward evaluation of the temperature dependence and finite-size effects, we also discuss an approach that combines our atomistic simulations with a lattice-site-resolved mean-field model.

A. Atomistic spin model incorporating anisotropic exchange interactions

In L1₀-FePt, Fe and Pt atomic layers are alternately stacked along the [001] direction^{16,17} (Figure 1 -(a)). As a result, the exchange coupling within a single Fe layer (in-plane direction, J_{\parallel}) is large due to direct Fe-Fe interactions, whereas the exchange coupling between adjacent Fe layers (out-of-plane direction, J_{\perp}) is weaker because it is mediated via Fe-Pt-Fe pathways¹⁹⁻²². Such pronounced exchange anisotropy is critical in the magnetization-reversal mechanism and thermal spin fluctuations.

In previous studies, L1₀-FePt has often been modeled-primarily for computational efficiency-by a "modified simple cubic" (modified-sc) structure that includes only the Fe degrees of freedom^{10,23} (Figure 1 -(b)). The DFT studies by Mryasov *et al.*²³ indicated that it is possible to reproduce the overall magnetic properties without explicitly including the Pt layers.

However, this modeling approach does not explicitly incorporate the substantial exchange anisotropy arising from the layered structure. In the design and development of HAMR media, the lateral grain dimension is carefully controlled, further underscoring the significance of anisotropy. Consequently, an anisotropic crystal model is essential for accurately evaluating finite-size effects in L1₀-FePt nanoparticles.

To address this issue, we further refine the modified-sc model by explicitly incorporating the anisotropic exchange interactions (J_{\parallel}/J_{\perp}) derived from DFT calculations. This approach enables us to accurately evaluate finite-size effects and capture the critical role of exchange anisotropy in L1₀-FePt nanoparticles.

The Hamiltonian for the anisotropic spin model can be written as:

$$H = -\frac{1}{2} \left[\sum_{\langle i,j \rangle_{\parallel}} J_{\parallel} (\mathbf{s}_i \cdot \mathbf{s}_j) + \sum_{\langle i,j \rangle_{\perp}} J_{\perp} (\mathbf{s}_i \cdot \mathbf{s}_j) \right] - k_u \sum_i (\mathbf{s}_i \cdot \hat{\mathbf{e}})^2 - \sum_i \mu_i (\mathbf{s}_i \cdot \mathbf{B}), \quad (1)$$

where $\sum_{\langle i,j \rangle_{\parallel}}$ denotes the summation over nearest-neighbor sites within the same atomic layer, and $\sum_{\langle i,j \rangle_{\perp}}$ denotes the summation over nearest-neighbor sites in adjacent layers. The quantity \mathbf{s}_i is the unit spin vector at site i , k_u is the uniaxial anisotropy constant, μ_i is the magnetic moment associated with the spin, and \mathbf{B} is the external magnetic field. By increasing the ratio J_{\parallel}/J_{\perp} , we explicitly account for differences between the in-plane and out-of-plane exchange couplings.

B. Extraction of the ratio of exchange constants via first-principles calculations

To quantitatively determine the ratio of intralayer (J_{\parallel}) and interlayer (J_{\perp}) exchange interactions in L1₀-FePt, we performed DFT calculations based on the methodology of Xiang *et al.*¹⁹. Concretely, using Quantum ESPRESSO²⁴, we mapped the total energies onto the classical Heisenberg model to extract the coupling constants. By switching the spin configurations between ferromagnetic (FM) and antiferromagnetic (AFM) states-either within a single atomic layer (AFM-intra) or between layers (AFM-inter) we calculated the following energy differences as schematically illustrated in Figure 5 :

$$\Delta E_{\parallel} = E(\text{AFM-intra}) - E(\text{FM}), \quad (2)$$

$$\Delta E_{\perp} = E(\text{AFM-inter}) - E(\text{FM}), \quad (3)$$

These energy differences (ΔE) are used to determine the exchange constant J by considering the number of spin sites (N) and the magnitude of each spin (S), consistent with the classical Heisenberg model. Specifically, by employing the energy difference between FM and AFM, one can define the total energy change of the spin system as the spin-spin interaction and thus obtain J , as shown in the following equation.

$$J = \frac{\Delta E}{NS^2}, \quad (4)$$

We obtained the respective values of J_{\parallel} and J_{\perp} from these calculations.

C. Temperature-dependent analysis via lattice-site-resolved mean-field modeling

To complement the atomistic simulations and rapidly estimate the temperature dependence of magnetization and the Curie temperature (T_c), we also employed a mean-field approximation model capable of resolving each lattice site separately²⁵. In this approach, the effective magnetic field at each site i , $\mathbf{B}_{\text{eff},i}$, is given by:

$$\mathbf{B}_{\text{eff},i} = \sum_j J_{ij} \langle \mathbf{s}_j \rangle + \mu \mathbf{B}, \quad (5)$$

where $\langle \mathbf{s}_j \rangle$ represents the thermally averaged spin at site j . Using the Langevin function to evaluate $\langle \mathbf{s}_j \rangle$, we can obtain a qualitative picture of the finite-temperature magnetization dynamics. Hence, at a coarse-grained level, this approach enables the estimation of T_c and its dependence on finite-size effects, which can be compared directly with simulations based on the atomistic spin model.

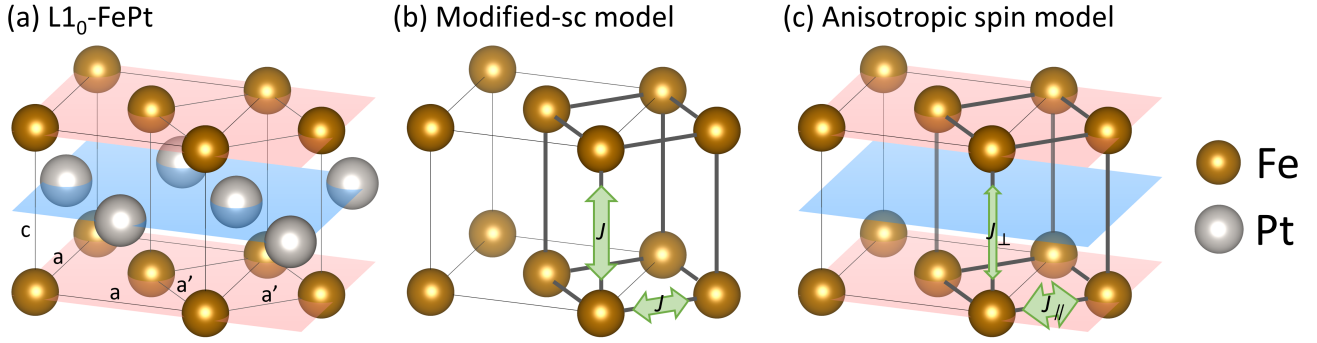


FIG. 1. (a) A schematic illustration of the $L1_0$ -FePt crystal structure. Fe and Pt atomic layers are alternately stacked along the [001] direction. (b) The modified-sc model proposed by Binh *et al.*¹⁰. In the Modified-sc Model, $L1_0$ -FePt is approximated solely by the Fe degrees of freedom and mapped onto a "simple cubic (sc)-like" lattice with dimensions $a' \times a' \times c$. This model simplifies the calculations by assuming isotropic Fe-Fe exchange interactions and unifying the treatment of exchange interactions. (c) The anisotropic spin model proposed in this study considers the in-plane Fe-Fe exchange interaction (J_{\parallel}) and the interlayer Fe-Fe exchange interaction (J_{\perp}) independently, thereby incorporating anisotropic effects arising from the crystal structure.

D. Calculation of Curie temperature using atomistic spin simulation

In this study, we analyzed the magnetic properties of FePt particles by partially modifying the atomic spin simulation software "VAMPIRE," developed by Evans *et al.*^{26–29}. VAMPIRE applies the Metropolis Monte Carlo method to determine the thermal equilibrium distribution of magnetization at temperature T and defines the Curie temperature T_c as the point at which the magnetization strength decreases sharply with increasing temperature.

More specifically, as the temperature is varied, the average magnetization length and the average magnetic susceptibility are obtained, and the following approximate equation, incorporating the critical exponent β , is used to determine T_c :

$$m(T) = \left\langle \sqrt{\sum_i \mathbf{S}_i} \right\rangle = (1 - T/T_c)^\beta, \quad (6)$$

Here, \mathbf{S}_i denotes the spin vector on site i , and $m(T)$ is the normalized magnetization length.

Additionally, for the determined T_c , we analyzed its particle size dependence by fitting the model represented by the following equation (Eq. 7) using the Finite-Size Scaling Law (FSSL)³⁰.

$$T_c(D) = T_{c0} \left(1 - x_{01} D^{-1/\nu_1} \right), \quad (7)$$

Where D is the particle width, T_{c0} is the Curie temperature for the bulk material, and x_{01} and ν_1 are fitting parameters. When both the width D and the height h of the particle are varied, this expression is extended accordingly.

III. RESULTS AND DISCUSSION

A. Evaluation of the Curie Temperature's Finite-Size Effect Using the Modified-sc Model

1. Overview and Significance

In this section, we reintroduce the "modified-simple cubic (modified-sc) model" introduced by Binh *et al.*¹⁰ and adapt it for our FePt nanoparticles to investigate the finite-size effect on the Curie temperature (T_c). Our objectives are (i) to verify whether this model, under our chosen conditions, can replicate the experimental trend of T_c as a function of particle size, and (ii) to clarify the model's limitations, which will form the basis for the extended approach presented in Part B.

2. Details of the Calculation Method

First, a "modified-sc" model proposed by Binh *et al.*¹⁰ was introduced. In this model, the simulation restricts the exchange interaction to only nearest neighbors, assuming it isotropic. The exchange interaction parameter J_{ij} is fitted such that the theoretical Curie temperature of bulk FePt (660 K)³¹ is reproduced. As a result, we obtained $J_{ij} = 6.303 \times 10^{-21}$ J/link. In addition, the normalized atomic spin moment U_s for the Fe atom and the uniaxial anisotropy constant K_u are set to $3.23 \mu_B$ and 2.63×10^{-22} J/atom, respectively³².

Although the modified-sc model significantly simplifies the treatment of exchange interactions, it still retains reasonable consistency with experimental and theoretical values. This model offers an extremely rational approach, especially for this study, which aims to evaluate the Curie temperature, magnetization distribution, and microscopic behavior across a variety of particle sizes, heights, and shapes in a rapid and qualitative manner.

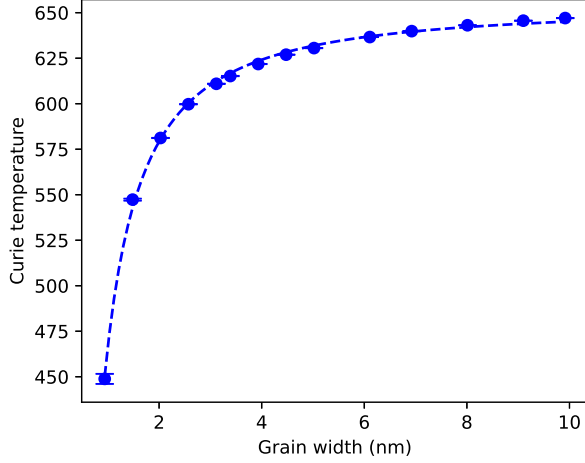


FIG. 2. Curie temperature as a function of particle width (with height fixed at 10 nm), along with the FSSL fitting. Around 5 nm, T_c begins to converge.

3. Calculation Results

In this study, simulations were carried out on square-column FePt crystal grains with various particle sizes and heights. Using the aforementioned FSSL, the particle size dependence of the Curie temperature was analyzed.

(1) Fixing the particle height at 10 nm and varying only the particle width

As shown in Figure 2, T_c increases sharply in the small particle diameter regime and tends to converge once the width is approximately 5 nm or greater. By applying FSSL for fitting, good agreement with the simulated data is achieved.

(2) Fixing the particle width at 6 nm or 8 nm and varying only the height

Figure 3 illustrates the behavior of T_c when the height is varied. The results for 6 nm and 8 nm widths both show similar trends, again in good agreement with the FSSL fitting. When normalized by the value of T_c at the height of 10 nm, the height-dependent variation becomes more evident.

From Figures 2 and 3, it is clear that changes in both the width and height of the particles yield size-dependent variations in T_c that follow the FSSL. Consequently, to incorporate width D and height h simultaneously into the finite-size effect, we perform the following extended fitting:

$$T_c(D, h) = T_{c0} \left(1 - x_1 D^{-1/\nu_1}\right) \left(1 - x_2 h^{-1/\nu_2}\right) \quad (8)$$

The seven fitting parameters obtained from this analysis are summarized in Table I.

In recent studies, it has been reported that real FePt particles with an average particle diameter of approximately 7-9 nm and $\sim 15\%$ particle-size distribution exhibit a Curie temperature dispersion σT_c of approximately 2%³³⁻³⁸. Similarly, in media evaluations within Resonac Corporation, it has been

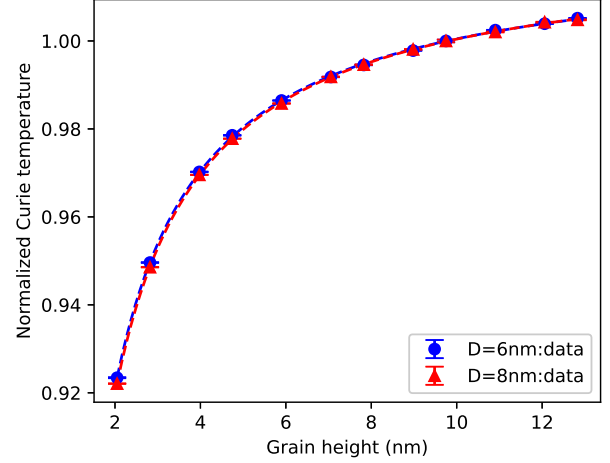


FIG. 3. Curie temperature versus particle height for widths of 6 nm and 8 nm, normalized to the value at $h = 10$ nm. Both examples exhibit similar behavior and fit well to the FSSL formula.

observed that, for instance, the sample in Table II has approximately a 2.5% spread in T_c , with a 20% spread in width and a 12% spread in height.

Using Eq. 8 in the present modified-sc model, we estimate the size-dependent T_c dispersion $\sigma T_{c, \text{size}}$ for the same particle size and height distribution referenced in Table II via:

$$\sigma T_{c, \text{size}} = \frac{T_c(\text{max}) - T_c(\text{min})}{2 \times T_c(\text{central})} \quad (9)$$

where $T_c(\text{max})$ and $T_c(\text{min})$ are the Curie temperatures for particles whose sizes are (mean \pm distribution), and $T_c(\text{central})$ is the value for the mean size. Under the conditions in Table II, the modified-sc model indicates that the average Curie temperature T_c was found to be 645.7 degrees, and the Curie temperature dispersion $\sigma T_{c, \text{size}}$ attributable to the size effect alone was approximately 0.8%, which is smaller than the experimentally observed 2.5

4. Discussion

In the first set of simulations, the size-effect contribution to $\sigma T_{c, \text{size}}$ was calculated to be 0.8%, considerably lower than the experimental value of 2.5%. If the size effect accounts for only $\sim 0.8\%$, then the remaining $\sim 1.7\%$ is presumably attributable to other factors, such as variations in ordering (particularly the degree of $L1_0$ layering) or lattice strain.

The significance of particle size effects on Curie temperature has been pointed out in various previous works⁶, and even if the estimated 0.7% itself appears small, it is still non-negligible. However, in $L1_0$ -FePt, the remarkable exchange anisotropy arising from the layered stacking of Fe and Pt along the [001] direction means that the in-plane (Fe-Fe) and out-of-plane (Fe-Pt-Fe) exchange strengths differ significantly^{16,17,19-22}. Because the modified-sc model treats

TABLE I. Representative fitting parameters for Eq. 8

T_{c0}	x_1	v_1	x_2	v_2
670.5 ± 1.4	0.247 ± 0.002	0.844 ± 0.018	0.194 ± 0.001	1.026 ± 0.013

TABLE II. Example of Resonac in-house media evaluation results

Average Width	Width Dispersion	Average Height	Height Dispersion	Curie Temperature	σT_c
7.8 nm	20%	10 nm	12%	650 K	2.5%

TABLE III. Example of the Vampire parameters for each level of anisotropy ratio in the anisotropic spin model

Anisotropy Ratio	J_{\parallel}	J_{\perp}
1.0	6.303×10^{-21}	6.303×10^{-21}
2.0	7.733×10^{-21}	3.867×10^{-21}
4.0	9.064×10^{-21}	2.266×10^{-21}
10.0	10.930×10^{-21}	1.093×10^{-21}

TABLE IV. The T_c dispersion ($\sigma T_{c,size}$) calculated for each anisotropy ratio in the anisotropic spin model

Anisotropy Ratio	$\sigma T_{c,size}$
1.0	0.8%
2.0	1.1%
4.0	1.4%
10.0	2.0%

these differences isotropically, it suggests that the finite-size effect on T_c may be underestimated.

Given these considerations, the following section proposes and evaluates a new spin model incorporating the anisotropy of intra-layer and inter-layer exchange constants, aiming to improve simulation accuracy.

B. Development of an Anisotropic Spin Model

1. Details of the Calculation Method

To address the issues identified in the previous section, we extended the modified-sc model to develop a new atomic spin model ("anisotropic spin model") that incorporates exchange anisotropy. We employed the VAMPIRE software to conduct atomic spin simulations, explicitly distinguishing between intra-layer and inter-layer exchange interactions. In this model, the intra-layer exchange interaction is denoted as J_{\parallel} and the inter-layer exchange interaction as J_{\perp} , and their ratio, J_{\parallel}/J_{\perp} , is referred to as the "Anisotropy Ratio," which can be freely adjusted. In this section, we set the anisotropy values to 1 (isotropic), 2, 4, and 10, and evaluated the variations in the Curie temperature for each setting. First, we calculated the T_c of the bulk crystal using the same procedure as the modified-sc model, obtaining approximately 685 K under the new parameter set. By adjusting the anisotropy ratio, the parameters listed in Table III reproduced the bulk T_c .

The spin magnetic moment ($3.23 \mu_B$) and uniaxial anisotropy constant (2.63×10^{-22} J/atom) are identical to those used in the modified-sc model.

2. Calculation Results

Using this new "anisotropic spin model," we calculated the T_c for cubic FePt particles as a function of their width and height, as described in Section A, and fitted the results using Eq. 8. Figure 4 shows the T_c behavior when (a) the particle height was fixed at 10 nm, and the width was varied, and (b) the particle width was fixed at 6 nm, and the height was varied. As the degree of anisotropy increases, the Curie temperature variation resulting from changes in particle width becomes significantly more pronounced. In contrast, the variation caused by changes in particle height remains relatively small. In each case, the T_c behavior followed the Finite Size Scaling Law (FSSL), reaffirming the finite size effect on T_c .

Furthermore, similar to Section A, we calculated the $\sigma T_{c,size}$ for each anisotropy level under the size dispersion conditions listed in Table II. The results are shown in Table IV. The results indicated that as the anisotropy increased, the impact of width variation on T_c dispersion also increased.

3. Discussion

This trend suggests that a larger $\sigma T_{c,size}$ can be achieved, closely aligning with the T_c dispersion observed in actual experiments. The calculations demonstrated that introducing anisotropic exchange interactions leads to more significant variation (dispersion) in Curie temperature due to size effects compared to the modified-sc model. When the exchange interactions are treated equivalently both within and between layers, as in the modified-sc model, the T_c dispersion tends to be significantly underestimated relative to experimental values. However, introducing anisotropy brings the results closer to reality. From these findings, it is clear that considering the strong exchange anisotropy inherent in the L1₀-FePt layered structure is essential for accurately estimating the Curie tem-

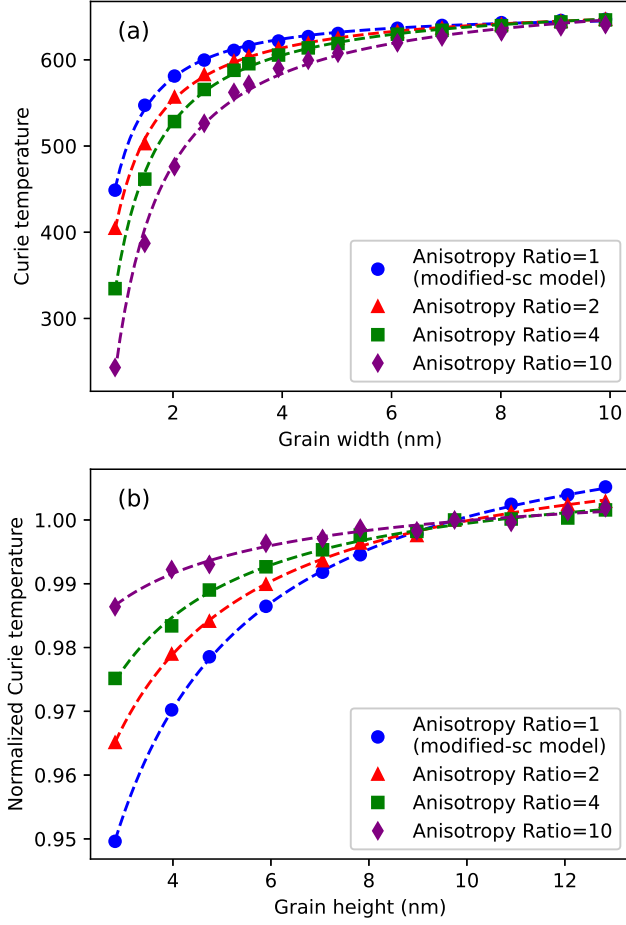


FIG. 4. Curie temperature variations for the anisotropic spin model of each anisotropy ratio: (a) Particle height is fixed at 10 nm while the width varies. (b) Particle width is fixed at 6 nm while the height varies (normalized to the value at $h = 10$ nm).

perature of nanoparticles. Therefore, in the next section, we aim to determine the precise ratio of intra-layer to inter-layer exchange constants (anisotropy ratio) for actual FePt crystals through first-principles (DFT) calculations. In the subsequent section, we will use these values to quantitatively demonstrate the contribution of size effects to the experimentally observed T_c dispersion.

C. Estimation of the Ratio of Anisotropic Exchange Constants from DFT Simulations

1. Computational Details

To evaluate the anisotropy ratio of exchange interactions in $L1_0$ -FePt, we performed DFT calculations using the Quantum ESPRESSO package²⁴. We extracted the difference between J_{\parallel} and J_{\perp} from these calculations. We employed the PBE exchange-correlation functional³⁹ and Projector Augmented-Wave (PAW) potentials⁴⁰ for Fe and Pt. The plane-wave cutoff

energies were set to 75 Ry for wavefunctions and 600 Ry for charge density, and we used a Monkhorst-Pack k-point mesh of $32 \times 32 \times 32$ points for Brillouin zone integrations. The supercell was constructed by alternating Fe and Pt atomic layers along the [001] direction, comprising a total of eight layers (16 atoms). Lattice constants and atomic positions were initialized using experimental data⁴¹, followed by energy minimization.

2. Calculation Results

To extract the exchange constants, we considered three collinear magnetic configurations and computed the total energy differences ΔE in each:

(A) FM: All Fe spins aligned along $+z$. (B) AFM-intra: Spins alternate between $+z$ and $-z$ within each atomic layer. (C) AFM-inter: Each layer is ferromagnetic internally, but adjacent layers alternate between $+z$ and $-z$.

Our calculations yielded:

$$\Delta E_{\parallel} = 0.003424 \text{ Ry} = 7.466 \times 10^{-21} \text{ J}, \quad (10)$$

$$\Delta E_{\perp} = 0.000486 \text{ Ry} = 1.056 \times 10^{-21} \text{ J}, \quad (11)$$

Given that there are eight Fe spins ($S = 1$) in the unit cell, the per-link exchange constants J_{\parallel} and J_{\perp} become:

$$J_{\parallel} = 9.333 \times 10^{-22} \text{ J/link}, \quad (12)$$

$$J_{\perp} = 1.320 \times 10^{-22} \text{ J/link}, \quad (13)$$

indicating that in-plane exchange J_{\parallel} is approximately 7.06 times stronger than out-of-plane exchange J_{\perp} .

3. Discussion

These results confirm that the in-plane Fe-Fe exchange is substantially stronger than the out-of-plane Fe-Pt-Fe superexchange. Similar conclusions have been reported in earlier work^{19–22}. The pronounced exchange anisotropy resulting from the layered structure of $L1_0$ -FePt strongly affects magnetization reversal and the finite-size behavior of T_c . In the present study, we incorporate this ratio ($J_{\parallel}/J_{\perp} \approx 7$) into the anisotropic spin model to quantitatively demonstrate the contribution of size effects to the experimentally observed T_c dispersion.

D. Application of the Anisotropic Exchange Interaction Ratio to the Anisotropic Spin Model

1. Parameter Settings

Based on the anisotropy ratio $J_{\parallel}/J_{\perp} \approx 7$ obtained in Section III C 2, we set the exchange interaction parameters for the

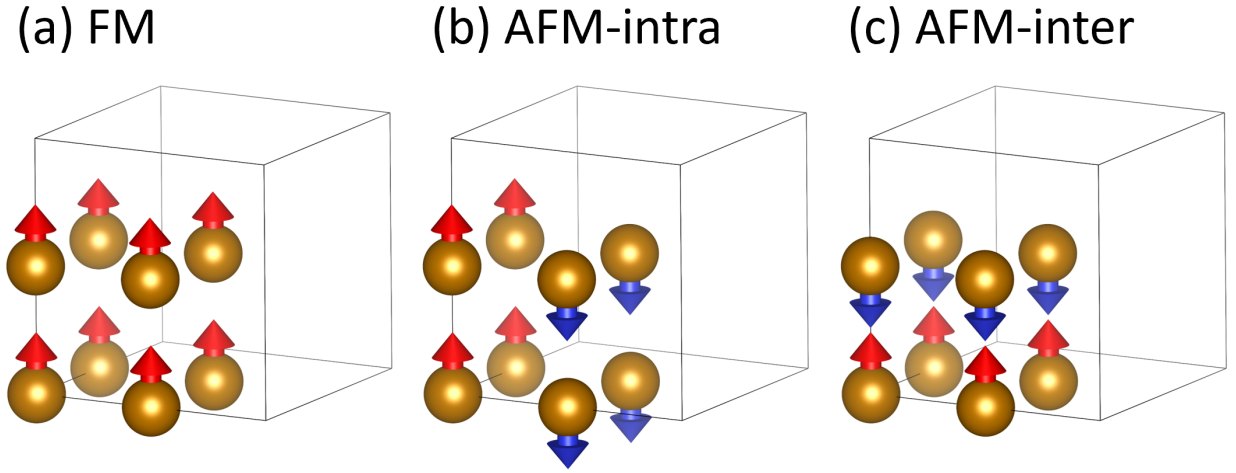


FIG. 5. Examples of the three cell configurations used to estimate the anisotropy of J : (a) FM, (b) AFM-intra, (c) AFM-inter. Fe atoms and their spins are illustrated; Pt atoms are omitted from the schematic. After structural optimization in QE, the total energies of each configuration were calculated.

TABLE V. Example of the Vampire parameters for the anisotropic spin model

Anisotropy Ratio	J_{\parallel}	J_{\perp}
7.06	10.033×10^{-21}	1.422×10^{-21}

anisotropic spin model. As before, the T_c for the bulk crystal was confirmed to be around 685 K. After adjusting the ratio $J_{\parallel} : J_{\perp} = 7 : 1$, we verified that the parameters in Table V reproduced the T_c of the bulk system.

2. Curie Temperature Calculation Results

Using this exchange interaction ratio $J_{\parallel}/J_{\perp} \approx 7$, we replicated the analysis performed in Section A by varying the width and height of cubic FePt grains, then fitted the resulting size-dependent T_c curves with Eq. 8. Figure 6 plots the observed T_c variation under the following conditions: (a) fixing the particle height to 10 nm while changing the width, and (b) fixing widths of 6 nm or 8 nm while varying the height. The data follow the FSSL trend in all cases, too.

Representative fitted parameters are summarized in Table VI. Comparing them with their counterparts in the modified-sc model (Table I), it is evident that x_1 and x_2 differ, indicating a change in how strongly T_c depends on size.

Moreover, for a size distribution like that in Table II, the average Curie temperature T_c was found to be 637.8 degrees and the size-dependent Curie temperature dispersion $\sigma T_{c,size}$ attributable to the size effect alone was found to be approximately 1.7%, implying that roughly 70% of the experimentally reported σT_c ($2 \sim 2.5\%$) could be explained by the size effect. The remaining $\sim 0.8\%$ is presumably due to other contributing factors such as chemical ordering and lattice strain.

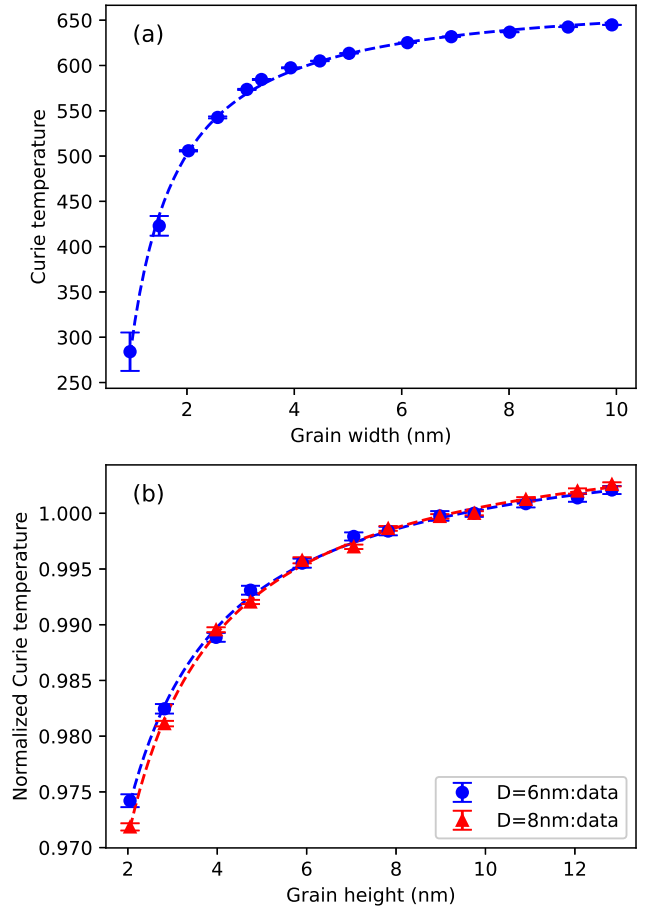


FIG. 6. Curie temperature variations for the anisotropic spin model: (a) Particle height is fixed at 10 nm while the width varies. (b) Particle width is fixed at 6 or 8 nm while the height varies (normalized to the value at $h = 10$ nm). In both cases, good agreement with the FSSL is observed.

TABLE VI. Example of fitting results for the anisotropic spin model

T_{c0}	x_1	v_1	x_2	v_2
691.5 ± 6.7	0.488 ± 0.006	1.045 ± 0.027	0.067 ± 0.001	1.107 ± 0.052

Nevertheless, the improved accuracy of the new model is apparent.

IV. CONCLUSION

In this study, we focused on the Curie temperature (T_c) dispersion of $L1_0$ -FePt nanoparticles. Specifically, (1) we employed a modified simple cubic (modified-sc) model to evaluate the decrease in T_c due to finite-size effects, and (2) constructed an anisotropic-sc model incorporating $L1_0$ -FePt exchange parameters to quantitatively reproduce and validate the variation in T_c caused by particle size dispersion. The principal findings, significance, and remaining challenges are summarized below.

A. Main Findings and Technical Significance

First, when only the finite-size effect was considered via the modified-sc model, the predicted T_c dispersion was approximately 0.8%, falling short of the experimentally reported value of around 2.5%. By contrast, our anisotropic-sc model, which captures the strong exchange anisotropy inherent in $L1_0$ -FePt, demonstrated that the sizeable in-plane exchange coupling enhanced spin correlation, increasing the overall T_c dispersion to 1.7%, thereby providing better agreement with experimental observations. This result demonstrates that including exchange anisotropy dramatically changes the finite-size effect in FePt nanoparticles, underscoring the critical importance of realistic modeling for accurately estimating T_c dispersion.

B. Industrial Implications

This study shows that particle size and size distribution strongly influence T_c dispersion. Therefore, applications that utilize large assemblies of nanoscale magnetic particles—such as HAMR media—require extremely careful size distribution management. On the other hand, even the proposed anisotropic-sc model retains a discrepancy of about 0.8% compared to experimental values, suggesting that combining additional measures such as enhancing the degree of chemical order and optimizing surface/boundary structures in the manufacturing process could further reduce T_c dispersion. Such an integrated approach is expected to offer a promising route toward simultaneously achieving thermal stability and high recording density.

C. Future Issues and Prospects

We confirmed that our newly proposed "anisotropic spin model" is highly promising as a more precise means of predicting T_c dispersion and magnetization characteristics in FePt nanoparticles. However, further inclusion of real material complexities—such as interactions beyond the nearest neighbor, inhomogeneities within particles, and the addition of other elemental species—will be necessary to achieve closer quantitative agreement with experimental data. Moreover, many issues remain, including the need to address local variations in magnetic properties induced by compositional changes near interfaces and quantify incoherent magnetization reversal modes. In future works, we plan to continue phase-by-phase verification with first-principles calculations and multi-scale simulations, aiming to develop models with broad applicability and high accuracy.

In summary, the anisotropic spin model that explicitly accounts for the pronounced exchange anisotropy in $L1_0$ -FePt nanoparticles proves to be highly beneficial for analyzing and designing next-generation HAMR media, wherein the layered structure notably amplifies finite-size effects. As such, our results are expected to aid both academic research and industrial development, providing guidelines for optimizing FePt-based magnetic materials in heat-assisted magnetic recording and high-efficiency spintronic applications.

¹D. Reinsel, J. Gantz, and J. Rydning, "Data age 2025: The evolution of data to life-critical," White Paper (International Data Corporation (IDC), 2017) accessed: 2023-10-04.

²D. Weller and A. Moser, "Thermal effect limits in ultrahigh-density magnetic recording," *IEEE Transactions on Magnetics* **35**, 4423–4439 (1999).

³S. N. Piramanayagam, "Perpendicular recording media for hard disk drives," *Journal of Applied Physics* **102**, 011301 (2007), https://pubs.aip.org/aip/jap/article-pdf/doi/10.1063/1.2750414/14993752/011301_1_online.pdf.

⁴J.-U. Thiele, S. Maat, and E. E. Fullerton, "Ferh/fept exchange spring films for thermally assisted magnetic recording media," *Applied Physics Letters* **82**, 2859–2861 (2003), https://pubs.aip.org/aip/apl/article-pdf/82/17/2859/18577791/2859_1_online.pdf.

⁵K. Hono and Y. K. Takahashi, "L10 fept granular films for heat-assisted magnetic recording media," *Ultrahigh Density Magnetic Recording*; Varvaro, G., Casoli, F., Eds., 246–277 (2016).

⁶D. Weller, G. Parker, O. Mosendz, E. Champion, B. Stipe, X. Wang, T. Klemmer, G. Ju, and A. Ajan, "A hamr media technology roadmap to an areal density of 4 tb/in²," *IEEE Transactions on Magnetics* **50**, 1–8 (2014).

⁷J. Waters, D. Kramer, T. Sluckin, and O. Hovorka, "Resolving anomalies in the critical exponents of FePt using finite-size scaling in magnetic fields," *Phys. Rev. Appl.* **11**, 024028 (2019).

⁸A. Lyberatos, D. Weller, and G. J. Parker, "Finite size effects in 110-fept nanoparticles," *Journal of Applied Physics* **114**, 233904 (2013), https://pubs.aip.org/aip/jap/article-pdf/doi/10.1063/1.4839875/13580327/233904_1_online.pdf.

⁹O. Hovorka, S. Devos, Q. Coopman, W. J. Fan, C. J. Aas, R. F. L. Evans, X. Chen, G. Ju, and R. W. Chantrell, "The curie temperature distribution of fept granular magnetic recording media," *Applied*

- Physics Letters **101**, 052406 (2012), https://pubs.aip.org/aip/apl/article-pdf/doi/10.1063/1.4740075/13900367/052406_1_online.pdf.
- ¹⁰N. T. Binh, S. Ruta, O. Hovorka, R. F. L. Evans, and R. W. Chantrell, "Influence of finite-size effects on the curie temperature of L1₀-FePt," Phys. Rev. B **106**, 054421 (2022).
- ¹¹A. Lyberatos, D. Weller, G. J. Parker, and B. C. Stipe, "Size dependence of the curie temperature of 110-fept nanoparticles," Journal of Applied Physics **112**, 113915 (2012), https://pubs.aip.org/aip/jap/article-pdf/doi/10.1063/1.4768260/15096302/113915_1_online.pdf.
- ¹²T. Tsuyama, "Driving force of atomic ordering in fe-pt alloys, investigated by density functional theory and machine-learning interatomic potentials monte carlo simulations," (2025), now printing.
- ¹³W.-H. Hsu and R. Victora, "Heat-assisted magnetic recording — micro-magnetic modeling of recording media and areal density: A review," Journal of Magnetism and Magnetic Materials **563**, 169973 (2022).
- ¹⁴J.-G. J. Zhu and H. Li, "Signal-to-noise ratio impact of grain-to-grain heating variation in heat assisted magnetic recording," Journal of Applied Physics **115**, 17B747 (2014), https://pubs.aip.org/aip/jap/article-pdf/doi/10.1063/1.4867607/14012954/17b747_1_online.pdf.
- ¹⁵H. Li and J.-G. Zhu, "The role of media property distribution in hamr snr," IEEE Transactions on Magnetics **49**, 3568–3571 (2013).
- ¹⁶A. Perumal, Y. K. Takahashi, and K. Hono, "Fept-c nanogranular films for perpendicular magnetic recording," Journal of Applied Physics **105**, 07B732 (2009), https://pubs.aip.org/aip/jap/article-pdf/doi/10.1063/1.3075986/14785641/07b732_1_online.pdf.
- ¹⁷D. Weller, A. Moser, L. Folks, M. Best, W. Lee, M. Toney, M. Schwickert, J.-U. Thiele, and M. Doerner, "High k/sub u/ materials approach to 100 gbits/in/sup 2/," IEEE Transactions on Magnetics **36**, 10–15 (2000).
- ¹⁸J.-G. Zhu and Y. Yan, "Incoherent magnetic switching of 110 fept grains," IEEE Transactions on Magnetics **57**, 1–9 (2021).
- ¹⁹H. J. Xiang, E. J. Kan, S.-H. Wei, M.-H. Whangbo, and X. G. Gong, "Predicting the spin-lattice order of frustrated systems from first principles," Phys. Rev. B **84**, 224429 (2011).
- ²⁰X. B. Liu and Z. Altounian, "Exchange interaction in 11-ordered fept and copt from first-principles," Journal of Applied Physics **109**, 07B762 (2011), https://pubs.aip.org/aip/jap/article-pdf/doi/10.1063/1.3564953/15070827/07b762_1_online.pdf.
- ²¹O. N. Mryasov, "Magnetic interactions in 3d-5d layered ferromagnets," Journal of Magnetism and Magnetic Materials **272-276**, 800–801 (2004), proceedings of the International Conference on Magnetism (ICM 2003).
- ²²J. B. Staunton, L. Szunyogh, A. Buruzs, B. L. Gyorffy, S. Ostanin, and L. Udvardi, "Temperature dependence of magnetic anisotropy: An ab initio approach," Phys. Rev. B **74**, 144411 (2006).
- ²³O. N. Mryasov, U. Nowak, K. Y. Guslienko, and R. W. Chantrell, "Temperature-dependent magnetic properties of fept: Effective spin hamiltonian model," Europhysics Letters **69**, 805 (2005).
- ²⁴P. Giannozzi, S. Baroni, N. Bonini, M. Calandra, R. Car, C. Cavazzoni, D. Ceresoli, G. L. Chiarotti, M. Cococcioni, I. Dabo, A. Dal Corso, S. de Gironcoli, S. Fabris, G. Fratesi, R. Gebauer, U. Gerstmann, C. Gougoussis, A. Kokalj, M. Lazzeri, L. Martin-Samos, N. Marzari, F. Mauri, R. Mazzarello, S. Paolini, A. Pasquarello, L. Paulatto, C. Sbraccia, S. Scandolo, G. Sclauzero, A. P. Seitsonen, A. Smogunov, P. Umari, and R. M. Wentzcovitch, "Quantum espresso: a modular and open-source software project for quantum simulations of materials," Journal of Physics: Condensed Matter **21**, 395502 (2009).
- ²⁵C. Penny, A. R. Muxworthy, and K. Fabian, "Mean-field modelling of magnetic nanoparticles: The effect of particle size and shape on the curie temperature," Phys. Rev. B **99**, 174414 (2019).
- ²⁶R. F. L. Evans, W. J. Fan, P. Chureemart, T. A. Ostler, M. O. A. Ellis, and R. W. Chantrell, "Atomistic spin model simulations of magnetic nanomaterials," Journal of Physics: Condensed Matter **26**, 103202 (2014).
- ²⁷R. F. L. Evans, U. Atxitia, and R. W. Chantrell, "Quantitative simulation of temperature-dependent magnetization dynamics and equilibrium properties of elemental ferromagnets," Phys. Rev. B **91**, 144425 (2015).
- ²⁸P. Asselin, R. F. L. Evans, J. Barker, R. W. Chantrell, R. Yanes, O. Chubykalo-Fesenko, D. Hinzke, and U. Nowak, "Constrained monte carlo method and calculation of the temperature dependence of magnetic anisotropy," Phys. Rev. B **82**, 054415 (2010).
- ²⁹D. A. Garanin, "Self-consistent gaussian approximation for classical spin systems: Thermodynamics," Phys. Rev. B **53**, 11593–11605 (1996).
- ³⁰J. Waters, A. Berger, D. Kramer, H. Fangohr, and O. Hovorka, "Identification of curie temperature distributions in magnetic particulate systems," Journal of Physics D: Applied Physics **50**, 35LT01 (2017).
- ³¹N. Kazantseva, D. Hinzke, U. Nowak, R. W. Chantrell, U. Atxitia, and O. Chubykalo-Fesenko, "Towards multiscale modeling of magnetic materials: Simulations of fept," Phys. Rev. B **77**, 184428 (2008).
- ³²M. Strungaru, S. Ruta, R. F. Evans, and R. W. Chantrell, "Model of magnetic damping and anisotropy at elevated temperatures: Application to granular fept films," Phys. Rev. Appl. **14**, 014077 (2020).
- ³³J.-G. Zhu, "The scaling of signal-to-noise in heat-assisted magnetic recording," IEEE Transactions on Magnetics **60**, 1–8 (2024).
- ³⁴N. Kulesh, A. Bolyachkin, I. Suzuki, Y. Takahashi, H. Sepehri-Amin, and K. Hono, "Data-driven optimization of fept heat-assisted magnetic recording media accelerated by deep learning tem image segmentation," Acta Materialia **255**, 119039 (2023).
- ³⁵A. Perumal, Y. K. Takahashi, and K. Hono, "L10 fept-c nanogranular perpendicular anisotropy films with narrow size distribution," Applied Physics Express **1**, 101301 (2008).
- ³⁶L. Zhang, Y. K. Takahashi, K. Hono, B. C. Stipe, J.-Y. Juang, and M. Grobis, "Feptag-c nanogranular film as thermally assisted magnetic recording (tar) media," IEEE Transactions on Magnetics **47**, 4062–4065 (2011).
- ³⁷B. S. D. C. S. Varaprasad, Y. K. Takahashi, J. Wang, T. Ina, T. Nakamura, W. Ueno, K. Nitta, T. Uruga, and K. Hono, "Mechanism of coercivity enhancement by ag addition in fept-c granular films for heat assisted magnetic recording media," Applied Physics Letters **104**, 222403 (2014), https://pubs.aip.org/aip/apl/article-pdf/doi/10.1063/1.4880655/13273596/222403_1_online.pdf.
- ³⁸K. Hono, Y. Takahashi, G. Ju, J.-U. Thiele, A. Ajan, X. Yang, R. Ruiz, and L. Wan, "Heat-assisted magnetic recording media materials," MRS Bulletin **43**, 93–99 (2018).
- ³⁹J. P. Perdew, K. Burke, and M. Ernzerhof, "Generalized gradient approximation made simple," Phys. Rev. Lett. **77**, 3865–3868 (1996).
- ⁴⁰P. E. Blöchl, "Projector augmented-wave method," Phys. Rev. B **50**, 17953–17979 (1994).
- ⁴¹S. Yuasa, H. Miyajima, and Y. Otani, "Magneto-volume and tetragonal elongation effects on magnetic phase transitions of body-centered tetragonal ferh(1-x)pt(x)," Journal of the Physical Society of Japan **63**, 3129–3144 (1994).